Journal of Power Sources 196 (2011) 5334–5341

Contents lists available at ScienceDirect

Journal of Power Sources

journal homepage: www.elsevier.com/locate/jpowsour

Characterization of high-power lithium-ion batteries by electrochemical impedance spectroscopy. I. Experimental investigation

D. Andre[a,*], M. Meiler[a], K. Steiner[a], Ch. Wimmer[a], T. Soczka-Guth[a], D.U. Sauer[b]

[a] Deutsche ACCUmotive, Neue Str. 95, D-73230 Kirchheim unter Teck, Germany
[b] Rheinisch Westfälische Technische Hochschule Aachen, Jägerstr. 17, D-52066 Aachen, Germany

ARTICLE INFO

Article history:
Received 15 June 2010
Received in revised form
20 December 2010
Accepted 22 December 2010
Available online 12 January 2011

Keywords:
Lithium-ion batteries
Electrochemical impedance spectroscopy

ABSTRACT

The influence of the operation conditions temperature and state of charge (SOC) on the performance of a commercial high-power lithium-ion cell is investigated by electrochemical impedance spectroscopy. Based on the results of several preliminary tests, measurements were run covering the complete range of automotive applications.

The cell impedance is presented and analyzed. A strong nonlinear temperature correlation is shown for all frequency ranges. Although the ohmic resistance is nearly unaffected by variation in SOC, the mass transport impedance reduces from 100% to 60% SOC and increases significantly again for lower SOCs.

1. Introduction

During the next years the automotive sector will face a challenging change from internal combustion engines to electrified power trains. The Boston Consulting Group for instance, expects the sale of 14 million cars with electric or hybrid power trains in 2020 [1]. However, this evolution will be a long and tough way accompanied by many technical issues. The main challenge will be to provide a battery which fulfils the requirements of the automotive sector: low weight, high mileage, long lifetime, high power and all that for a low price.

At the moment, lithium-ion battery is the only available battery technology which is able to comply with all those requirements. The first series-produced hybrid electric vehicle (HEV) equipped with lithium-ion cells was launched by Mercedes Benz with the S400 Hybrid in 2010, reducing the CO_2 emission by 20% [2]. Several other car manufacturers will follow in the next years [3].

One of the main tasks of the battery in HEVs is to provide a sufficient amount of power for acceleration, thus reducing the CO_2 emission at all operating conditions. The performance of every battery cell is defined by their open circuit cell voltage (OCV), nominal cell capacity C_N and impedance Z. Whereas OCV and cell capacity show only a low temperature dependency, the impedance is strongly temperature as well as state of charge (SOC) dependent [4]. Therefore, it is essential to have a precise knowledge of the cell behaviour at all operating conditions in order to receive an energy- and cost-optimal design.

Two approaches are known to investigate the dynamic behaviour of a cell: first electrochemical impedance spectroscopy (EIS) and second the measurement of a voltage response after a DC pulse. This study uses EIS measurements to investigate the influence of the operating conditions temperature T and state of charge on the cell impedance in a wide frequency range. Thus, different processes in the cell can be observed and interpreted with the aim to get an improved understanding of lithium-ion cells.

2. Theory of EIS for lithium-ion batteries

EIS is a widely used experimental method to gain a deeper insight into electro-chemical systems. In the last years EIS was applied by several research groups [5–8] to lithium-ion cells. As mentioned the advantage of EIS is the measurement in a wide frequency range, which offers the possibility to draw conclusions about internal processes with different time constants.

These time constants are explained in Fig. 1 by applying a current pulse on a cell.

If neglecting all internal processes, the cell voltage drops linear like described by Ohm's law. However, in reality the voltage declines in three parts [9]. The first one is characterized by the ohmic loss and takes effect without any time delay after the current pulse. Second, the voltage loss caused by charge transfer runs after a time delay, determined by the double layer capacity, into a steady voltage. Third, the

* Corresponding author at: Deutsche ACCUmotive GmbH & Co. KG, Entwicklung Zelltechnologie, Neue Straße 95, 73230 Kirchheim unter Teck, Germany.
Tel.: +49 015158605924.
E-mail address: dave.andre@daimler.com (D. Andre).

0378-7753/$ – see front matter © 2011 Elsevier B.V. All rights reserved.
doi:10.1016/j.jpowsour.2010.12.102

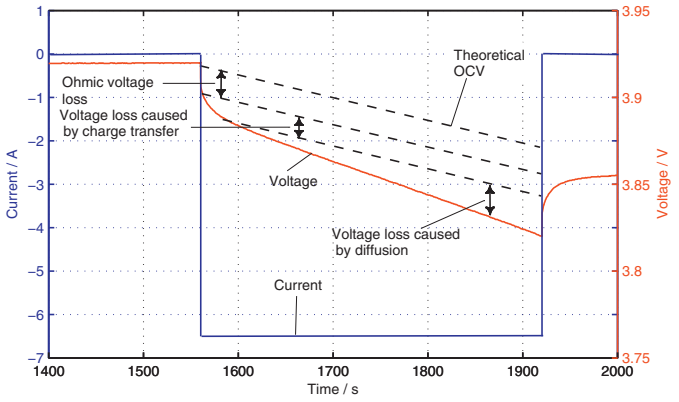

Fig. 1. Voltage response of a lithium-ion cell after a current pulse.

voltage losses caused by insufficient diffusion of lithium ions into the active material increases till the end of the voltage drop.

The general principle of the EIS method is to apply a sinusoidal signal and measuring the characteristic response from the cell which depends on the cell impedance. The input signal can either be current (galvanostatic) or voltage (potentiostatic). A typical current and voltage curve for EIS has the form of a Lissajous figure. One of these recorded figures is illustrated in Fig. 2.

The voltage $u(t)$ and the phase shift ϕ are recorded as responses of the measurements. By using the following equation:

$$\underline{Z} = \frac{u(t)}{i(t)} = \frac{\hat{U}\cdot\sin(\omega t)}{\hat{I}\cdot\cos(\omega t-\phi)} = \left|\underline{Z}\right|\cdot\frac{\sin(\omega t)}{\cos(\omega t-\phi)} \quad (1)$$

where $\hat{U}$ is the amplitude of the voltage signal, $\hat{I}$ is the amplitude of the current signal, ω is the angular frequency, ϕ is the phase shift and $|\underline{Z}|$ is the absolute value of the impedance, a correlation to the impedance Z can be calculated. Furthermore, it is possible to separate the impedance in a real part Z' and an imaginary part Z'' by using ϕ again:

$$Z' = \left|\underline{Z}\right|\cdot\cos(\phi) \quad (2)$$

$$Z'' = \left|\underline{Z}\right|\cdot\sin(\phi) \quad (3)$$

$$\left|\underline{Z}\right| = \sqrt{Z'^2+Z''^2} \quad (4)$$

Finally, Z' and Z'' can be displayed in a Nyquist plot in order to visualize the influence of the parameters. Nyquist plots are the first choice for EIS measurements but have the fundamental disadvantage, that Nyquist plots do not contain information about time. Therefore, it is not possible to identify the frequency of the measured points. In order to avoid this problem, Bode plots are used in this work too.

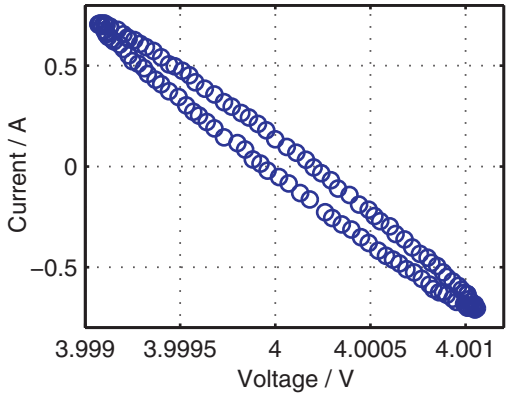

Fig. 2. Recorded Lissajous figure of current and voltage at 24 °C and 100% SOC for a frequency of 50 Hz.

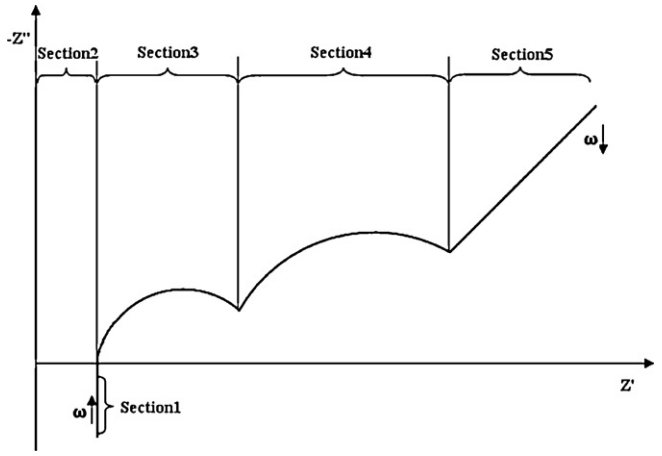

Fig. 3. Schematic impedance spectrum in a Nyquist plot for lithium-ion cells.

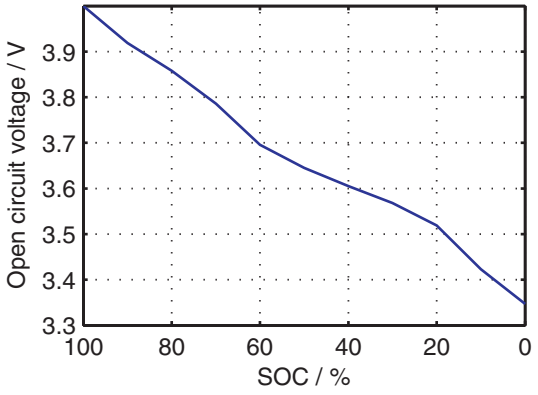

Fig. 4. Measured open circuit voltage as a function of SOC.

Impedance spectra of lithium-ion cells show a characteristic behaviour in a Nyquist plot. Fig. 3 presents this theoretical curve. Five different sections exist, which in literature are related to particular processes. However, the interpretation of spectra is difficult and many processes are still understood insufficiently. The sections and the assumed responding kinetic processes are explained in more detail:

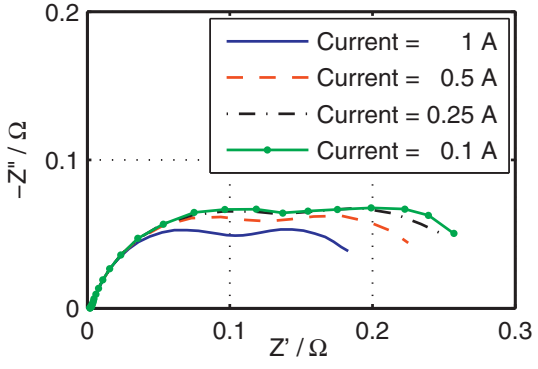

Fig. 5. Effect of current on impedance spectra at −30 °C and 60% SOC.

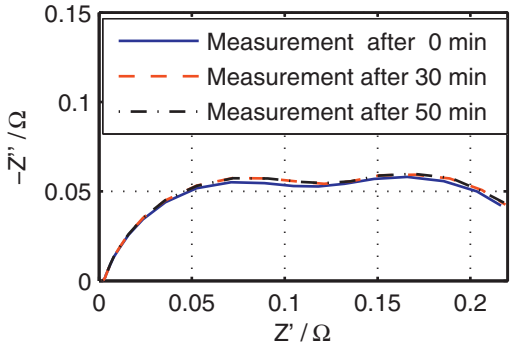

Fig. 6. Effect of pause time after SOC variation (ΔSOC = 10%) on impedance spectra at −30 °C and 50% SOC.

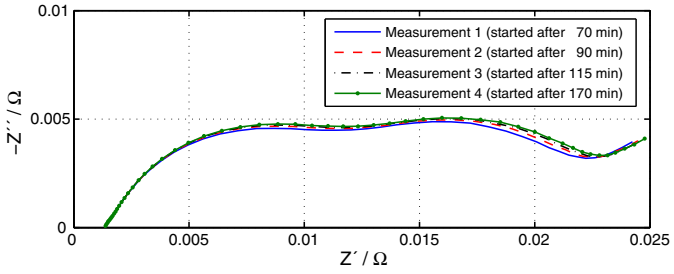

Fig. 7. Effect of pause time after temperature variation (ΔT = 30 K) on impedance spectra at −10 °C and 60% SOC.

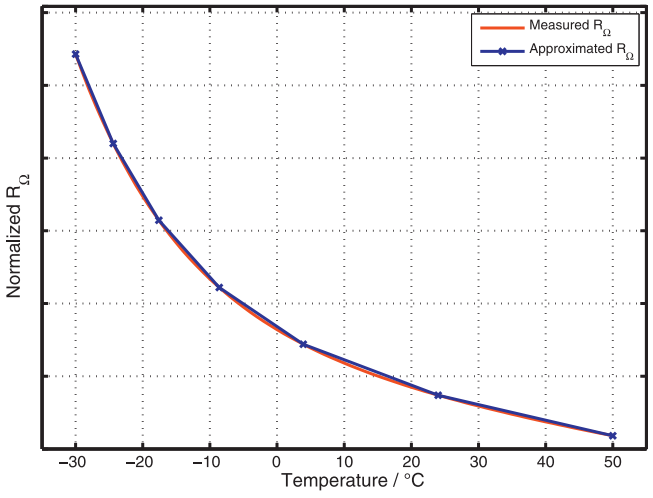

Fig. 8. Approximation of internal cell resistance R_Ω by seven points as a function of temperature.

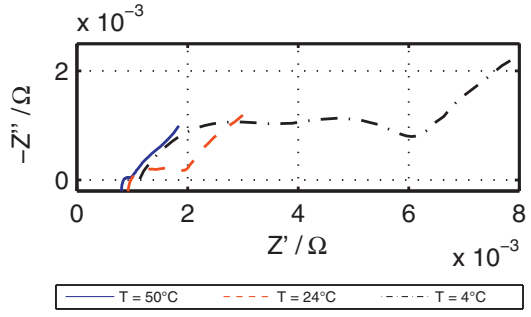

Fig. 9. Impedance spectra for positive temperatures at 60% SOC.

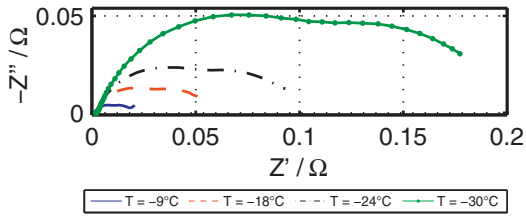

Fig. 10. Impedance spectra for negative temperatures at 60% SOC.

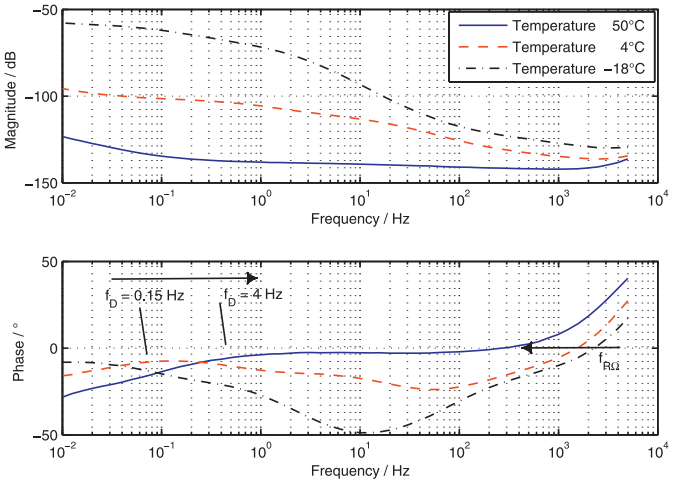

Fig. 11. Bode plot of EIS measurements at 60% SOC.

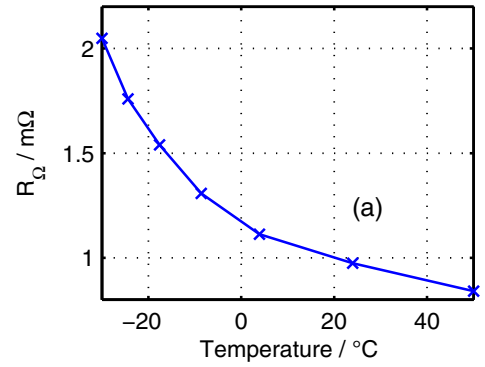

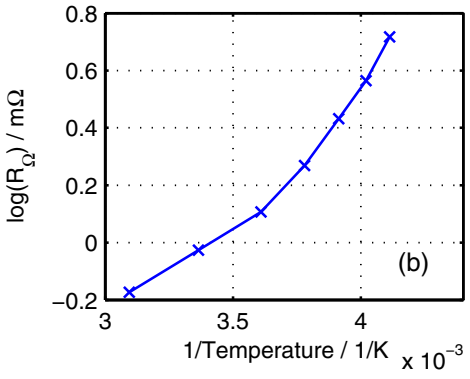

Fig. 12. Influence of temperature (a) on R_Ω at 60% SOC and (b) Arrhenius plot of R_Ω.

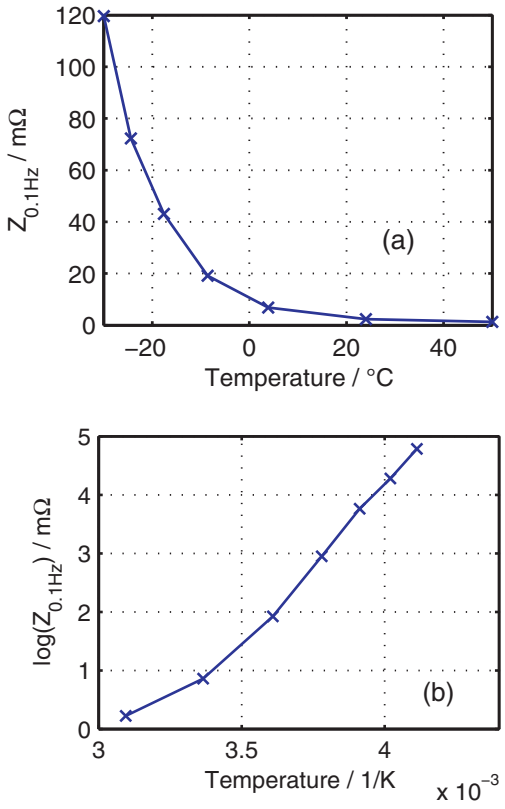

Fig. 13. Influence of temperature (a) on $Z_{0.1\,Hz}$ at 80% SOC and (b) Arrhenius plot of $Z_{0.1\,Hz}$.

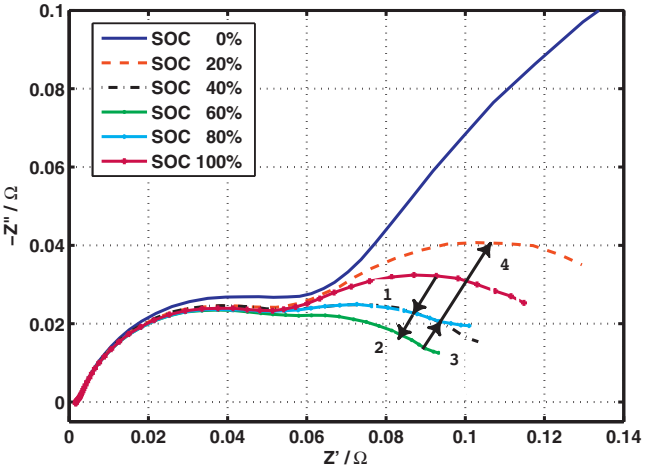

Fig. 14. Impedance spectra for different SOCs at $T = -24\,^{\circ}C$.

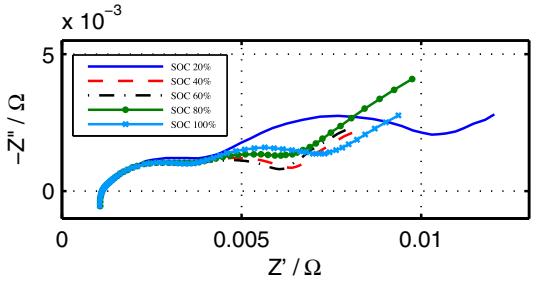

Fig. 15. Impedance spectra for different SOCs at $T = 4\,^{\circ}C$.

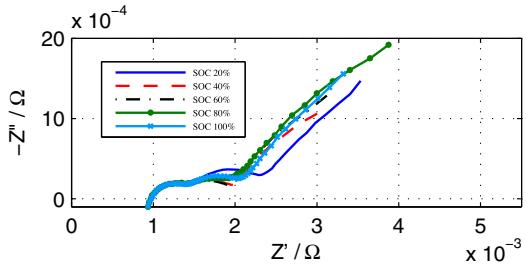

Fig. 16. Impedance spectra for different SOCs at $T = 24\,^{\circ}C$.

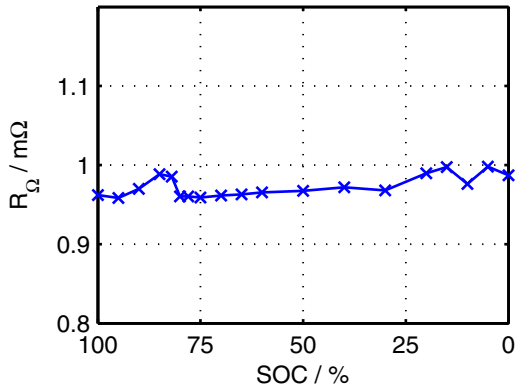

Fig. 17. Influence of SOC on R_Ω at 24 °C.

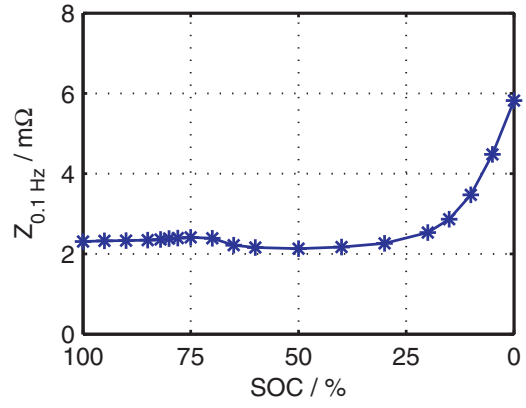

Fig. 18. Influence of SOC on $Z_{0.1\,Hz}$ at 24 °C.

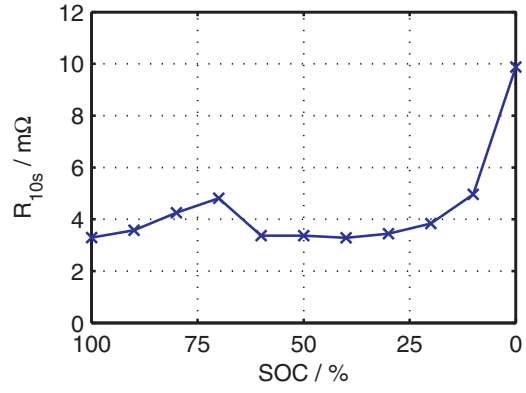

Fig. 19. Influence of SOC variation on $R_{10\,s}$ at 23 °C.

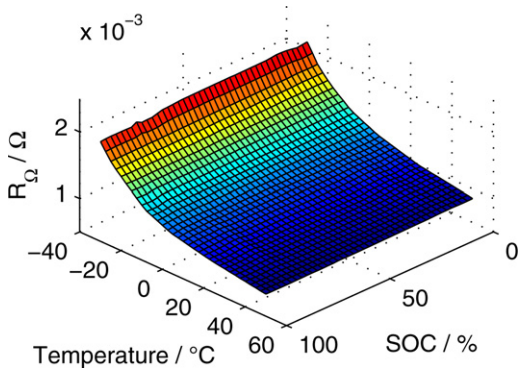

Fig. 20. Influence of SOC and temperature variation on R_Ω.

- *Section 1*. At very high frequencies the spectrum shows inductive behaviour caused by inductive reactances of metallic elements in the cell and wires
- *Section 2*. Ohmic resistance R_Ω of the cell at the intersection with the real axis, sum of the resistances of current collectors, active material, electrolyte and separator
- *Section 3*. First semi-circle associated typically with the solid electrolyte interface (SEI) [10] and is formed during cycling on the surface of the anode [11]
- *Section 4*. Second semi-circle representing the double layer capacity and charge transfer resistance at the electrodes [12,13]
- *Section 5*. Diffusion processes in the active material of the electrodes at very low frequencies [14]

Measured spectra often show variations of this theoretical curve. Often the number of circles is just one, the inductive behaviour at high frequencies is a loop instead of a line in consequences of the skin effect of the material [9] or the diffusion line has an angle unequal 45°. As described EIS measurements offer the chance to identify and investigate the influence of electrochemical processes. In order to avoid misinterpretations through similar time constants of both electrodes, results often have to be clarified by additional half cell experiments [12].

3. Experimental setup

All tests were run with the VL6P, a commercial 6.5 Ah high-power lithium-ion cell from Saft S.A. A cylindrical cell optimized for the use in hybrid vehicles, which allows maximum current pulses up to 250 A.

The cathode of this cell consists of a nickel–cobalt–aluminium (NCA) composition, which is known for high cycle stability, sufficient power at low temperatures, e.g. for cold-cranking, as well as a long calendar lifetime [15]. The anode of this cell consists of graphite, the standard material of negative electrodes in lithium-ion cells. Between both electrodes a 20 μm thick polymer separator and a liquid organic solvent based electrolyte with several additives are placed. The electrical and mechanical parameters of the VL6P cell are provided in Tables 1 and 2 respectively [16].

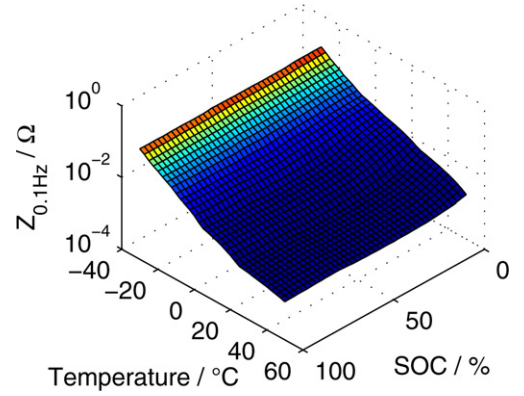

Fig. 21. Influence of SOC and temperature variation on $Z_{0.1\,Hz}$.

Table 1
Electrical parameter of VL6P cell.

Nominal voltage	3.6 V
Nominal capacity	6.5 Ah (C/3, 4 V)
Power	720 W
Maximum current	250 A
Energy density	67 Wh kg^{-1}
Power density	2060 W kg^{-1}

Every battery cell is characterized by its typical OCV curve. The measured OCV curve is presented in Fig. 4 and shows an almost linear behaviour except a kink at about 60% SOC. This kink seems to be a consequence of the specific cell chemistry and is already visible for a very similar cell in Johnson et al. [17].

All described experiments were accomplished on a measuring computer by BaSyTec GmbH and by a software for monitoring, controlling and recording the whole measuring process. Charging and discharging of the cell were realized by BaSyTecs power electronic HPS. Moreover this power electronic was monitoring:

- Voltage
- Current
- Temperature on the surface of the cell
- Temperature in the climatic chamber
- Additional voltage for safety aspects

In order to heat the cell to the desired temperature, a climate chamber 4018VC^3 by Vötsch Industrietechnik GmbH was used. Thus, a temperature range from −42 °C to 180 °C could be realized, including the entire temperature range of lithium-ion cells in automotive applications.

4. Preliminary tests

In order to gain optimized test conditions, several systematic preliminary tests were run. The goal of these tests was to answer following open points:

- Necessary frequency for EIS measurements
- Reasonable current amplitude
- Length of pause time after temperature variation
- Length of pause time after SOC variation
- Maximum C-rate (current for discharging the nominal cell capacity within 1 h) in consideration of test temperature
- Number of measuring points per frequency decade
- Optional application of a DC-offset

The sampled frequency range has to include at minimum the Z'-interception for the determination of R_Ω at high frequencies and all capacitive processes at low frequencies. By variation of the fre-

Table 2
Mechanical parameters of VL6P cells.

Cylindrical cell casing made of Al	
Length	145 mm
Diameter	38 mm
Volume	160 cm^3
Weight	350 g

Table 3
Parameters of impedance measurement for VL6P cell.

Parameter	Parameter range
Frequency, f	10 mHz–5 kHz
Current, I_{eff}	0.5 A
Pause time after ΔSOC	15–90 min
Pause time after ΔT	3 h
C-Rate	0.02–1C
Number of frequencies per decades	10
DC - offset	0 A

quency, the necessary range was determined and is listed in Table 3. This range was used for all measurements.

Several EIS tests with variation of the current amplitude from 0.1 A to 1 A were run to determine the current influence on the impedance spectrum. The results are shown in Fig. 5. A shrinking of both semi-circle diameters can be observed with rising current. The reason for this phenomenon is an increased cell temperature at higher current, having a strong influence on the spectrum as Section 6.1 will show in detail. No temperature increase was detected during the measurement for a current of 0.25 A and 0.5 A, but an increase of 0.4 K was observed at 1 A. This raise in temperature seems small, but especially for cylindrical cells the internal temperature raise can be a multiple of the increase at the cell surface and even a small temperature rise distorts the EIS measurement at very low temperature. At room temperature no influence of current on the impedance spectrum was observed. Small currents signals are just producing small and therefore difficult to measure voltage responses. Consequently, a current of 0.5 A was chosen for all tests at which the amount of generated heat is still low and the response is clear.

To determine the necessary pause time until a steady state is reached after adjusting the SOC, several EIS tests with different time-lags after a discharge were run. One of the results is given in Fig. 6 for a temperature of −30 °C.

When the impedance spectrum is measured directly after a SOC variation of 10% and half an hour later, a shift of the spectrum can be observed. The reason of this shift is a relaxation of the cell towards the OCV after every charge or discharge. If the measurement is carried out 50 min after the variation, the shift of the spectrum is only minimal compared to the spectrum measured after half an hour. Depending on temperature and SOC, different pause times were adhered from 15 to 90 min.

A similar approach was used to analyse the influence of temperature variation. The result is displayed in Fig. 7.

For a temperature change from 20 °C to −10 °C a drift of the spectrum can be seen during the first 2 h which vanishes afterwards. Then, the cell is tempered and the system has reached a thermal steady state. Therefore, a pause time of 3 h was adhered in all tests. Since the climate chamber needs additional time for heating, the pause time was just started when the sensors at the cells had reached the set-point temperature.

For discharging the cell to the desired SOC with a maximum C-rate under the constraints of not reaching the end of discharge voltage or producing high amounts of heat, different C-rates were determined in the range of 0.02–1 C depending on SOC and temperature.

The number of measuring points depends on the impedance curve and the number of parameters which have to be identified for an equivalent circuit model. In case an insufficient number of measuring points is recorded, the parameter estimation will be instable and the impedance curve can not be reproduced properly. Therefore ten points were recorded per decade, resulting in 58 points in total for every test.

In literature [5,18,19] EIS measurements with DC-offset can be found. However, in these experiments no offset was used. The reason for this decision is on the one hand a non negligible SOC shift for an average testing time of 25 min and on the other hand a triplication of test effort for additional positive and negative DC-offsets. Moreover test conditions exist where offsets are not acceptable, such as charging at low temperature or discharging at low SOC.

Table 4
Investigated parameter cross for temperature and SOC.

T (°C)	SOC (%)																	
	100	95	90	85	75	70	65	60	50	40	30	25	20	15	10	5	0
−30																	
−10																	
20																	
40																	
50																	

Table 5
Determined points of temperature for EIS measurement.

Measurement points of temperature (°C)						
50	24	4	−9	−18	−24	−30

5. Test planning

In order to obtain a maximum of information from a minimum of experiments, the influence of temperature at constant SOC and the influence of SOC at constant temperature were studied. The investigated parameter cross is provided in Table 4.

Based on the results, measurement points were determined to characterise the cell sufficiently. In intervals where large variations of the measurement results were observed, additional tests were planned. However, in case of a nearly linear dependency, less measurement points were taken. The overall trend of temperature influence on internal cell resistance R_i can be described by an exponential function as Fig. 8 illustrates.

By the method of least squares between the measured R_i and a linear interpolated one by means of a lookup table, the optimal supporting points were determined and are listed in Table 5.

As a result of these tests, impedance measurements were carried out for seven different temperatures and for eighteen different SOCs. The SOC range was spaced with a distance of five per cent at high and low SOC, and ten per cent in the medium SOC range. The determined measurement matrix is shown in Table 6 and contains in total 119 measuring points.

6. Experimental results

6.1. Influence of temperature

As shown in Table 5, the influence of temperature was investigated at seven supporting points. The temperature influence on the impedance spectrum is as strong as expected. Since the spectra-ranges differ extremely with temperature, the results for positive

Table 6
Measurement matrix.

T (°C)	SOC (%)																	
	100	95	90	85	75	70	65	60	50	40	30	25	20	15	10	5	0
−30																	
−24																	
−18																	
−9																	
4																	
24																	
50																	

temperatures are displayed in Fig. 9 and for negative temperatures in Fig. 10.

For lower temperatures a spread of both semi-circles can be observed, a similar trend to Linzen [20]. This spread is a consequence of slower chemical processes at low cell temperatures and corresponding higher cell impedance. Especially diffusion processes strongly depend on temperature, which is represented in Fick's law by the diffusion coefficient. Both spreads can be interpreted by the processes explained in Section 2. The first circle is dominated by the SEI. At a decreased thermal energy ions have a lower kinetic energy, therefore the ions move slower through the interface and accordingly the resistance is higher. The same effect can be applied to explain the second circle which is a mix of charge transfer and diffusion processes. Again both processes are functions of temperature and the resistance is thus higher.

In addition, for elevated temperatures both semi-circles grow together and can not be distinguished anymore. That means the time constants of the internal processes get similar and a separation is not possible anymore. At decreasing temperature, the value of the intersection with the real axis, i.e. the ohmic resistance R_Ω, is rising.

Since no information about time is included in these graphics, Bode plots for three different temperatures at a SOC of 60% are presented in Fig. 11. Three interesting points can be observed. First, all three temperatures show a very similar inductive behaviour, but are diverging at lower frequency and have therefore different capacitive behaviours. This similar trend at higher frequencies was expected since the inductivity of a cell is mainly contributed by the current conduction which is independent of temperature. Second, the zero intersection of the real axis ($\phi = 0$) is occurring at lower frequencies for higher temperatures. Third, the frequency where the diffusion process starts is shifting to lower values for decreasing temperatures and has not even started at 0.01 Hz for −18 °C. In addition, it is obvious that both semi-circles are well-defined in the medium temperature range, but for 50 °C the phase of the impedance is continuously rising. Very similar behaviours were found for other SOCs and are therefore not discussed.

In Fig. 12 the influence of temperature only on the ohmic resistance R_Ω is shown for a constant SOC. R_Ω shows a nonlinear behaviour and has a three times higher value at −30 °C than at 50 °C, emphasising the strong influence of operating temperature on cell resistance and consequently cell performance. This issue becomes even more obvious by looking at the sum of the impedance parts as introduced in Eq. (4) at a frequency of 0.1 Hz at a typical SOC of HEVs with 80%. Hereby even an exponential increase by a factor of one hundred can be seen within the temperature range of 3–4 °C in Fig. 13. Additional Arrhenius plots in Fig. 12(b) and Fig. 13(b) indicate the exponential function of both values with temperature. However, both curves suggest that above 20 °C the influence of temperature gets smaller and the curve runs into a steady state.

6.2. Influence of state of charge

Also the SOC of the cell has a strong influence on the impedance spectrum as Fig. 14 shows for −24 °C, Fig. 15 for 4 °C and Fig. 16 for 24 °C.

For all cases the first semi-circle shows no significant SOC dependency. However, the second semi-circle is spreading strongly with declining SOC which can especially be observed for SOCs lower than 30%. Therefore the resistance of the SEI is not a function of the SOC, however charge transfer and diffusion resistance are higher if the cell voltage is lower.

At low temperatures an interesting effect on the diameter of the second semi-circle, which is also present at high temperatures, can be seen clearly. From 100 to 60% SOC the diameter of the second semi-circle decreases (as in Fig. 14), but increases again at lower SOCs. This effect was not found in literature [9,19] and is therefore probably due to the specific chemistry of the cell. In contrast to temperature just a low impact of SOC on the ohmic resistance was measured and is displayed in Fig. 17. A slight increase, which seems to be linear, can be observed with decreasing SOC. However, looking again at the sum of the impedance at a frequency of 0.1 Hz an exponential rise can be observed as it is illustrated in Fig. 18. A very similar dependency can be seen for the cell resistance measured by the voltage response after a ten seconds current pulse as visible in Fig. 19. Both figures show the same exponential rise towards low state of charges. Moreover, both curves show an interesting bump from 60 to 90% SOC, possibly a consequence of the kink in the OCV curve of Fig. 4. However, this bump as well as the kink gets smaller during cell aging and vanish finally.

7. Summary

In the last sections the influence of the main battery operating conditions -temperature and state of charge- on cell impedance and thus cell performance was shown for the mass produced 6.5 Ah VL6P cell.

Concerning temperature a very strong spread of both semi-circles was observed for decreasing temperatures, indicating an increase of SEI resistance and double layer resistance with decreasing thermal energy. In addition, the frequencies of the chemical processes were investigated. It was found out that the intersection with the real axis occurs at lower frequencies for higher temperatures, but that impedance caused by diffusion phenomena starts at higher frequencies with increasing temperature. Moreover, the strong impact of temperature on the ohmic resistance R_Ω was shown. The resistance almost triples within the temperature range of automotive applications.

Typical vehicle operations are in the range of a few seconds and therefore comparable with impedance values at 0.1 Hz. This additional consideration of charge transfer and diffusion yields into an even one hundred times higher impedance.

The consequences are an insufficient amount of power at low temperatures in the vehicle, resulting in either higher fuel consumption or even issues for cranking if no additional starter battery is provided. Therefore the battery and drive train have to be designed in such way that even at low temperature all functionalities are guaranteed.

Additionally, the state of charge of a cell showed a strong effect on the impedance spectrum affecting mainly the second semi-circle, which is especially visible for SOCs below 30%. Since this semi-circle is typically associated with the charge transfer and diffusion resistance, a significant increase can be deduced from these observations. In contrast to temperature, the effect of SOC variation on R_Ω is rather small. Thus, the measurement of the internal resistance is not suited as an online state of charge indicator of this cell. The low impact of SOC can also be seen in the summarizing characteristic diagram of R_Ω in Fig. 20. It is obvious that the main influence is caused by temperature and only a small SOC influence can be guessed at the edge. For the impedance at 0.1 Hz an exponential influence of SOC was presented. Although this effect is again just small in comparison to the effects of the temperature as the logarithmical plot in Fig. 21 indicates, a factor of three is not negligible for an operation strategy.

In the next step these measured EIS data should be used for battery modelling. Aim of this approach is the prediction of battery voltage and therefore battery performance under all operating conditions.

References

[1] A. Dinger, R. Martin, X. Mosquet, M. Rabl, D. Rizoulis, M. Russo, G. Sticher, Batteries for Electric Cars: Challenges, Opportunities,

and the Outlook to 2020, The Boston Consulting Group, 2010. http://www.bcg.com/documents/file36615.pdf.
[2] A.G. Daimler, Umwelt-Zertifikat für den S 400 Hybrid, Tech. Rep. Life Cycle, Stuttgart, 2009. http://www3.mercedes-benz.com/fleet-sales/de/umweltzertifikat_s_400.pdf.
[3] F. Nemry, G. Leduc, A. Muñoz, Plug-in hybrid and battery-electric vehicles: State of the Research and Development and Comparative Analysis of Energy and Cost Efficiency, Tech. Rep., Institute for Prospective Technological Studies, Sevilla, 2009. http://ftp.jrc.es/EURdoc/JRC54699_TN.pdf.
[4] P. Nelson, I. Bloom, K. Amine, G. Henriksen, J. Power Sources 110 (2) (2002) 437–444.
[5] M. Itagaki, N. Kobari, S. Yotsuda, K. Watanabe, S. Kinoshita, M. Ue, J. Power Sources 148 (2005) 78–84.
[6] U. Tröltzsch, O. Kanoun, H.-R. Tränkler, Electrochim. Acta 51 (8–9) (2006) 1664–1672.
[7] R.G. Jungst, G. Nagasubramanian, H.L. Case, B.Y. Liaw, A. Urbina, T.L. Paez, D.H. Doughty, J. Power Sources 119–121 (2003) 870–873.
[8] C.H. Chen, J. Liu, K. Amine, J. Power Sources 96 (2) (2001) 321–328.
[9] A. Jossen, J. Power Sources 154 (2) (2006) 530–538.
[10] M.D. Levi, K. Gamolsky, D. Aurbach, U. Heider, R. Oesten, Electrochim. Acta 45 (11) (2000) 1781–1789.
[11] J. Vetter, P. Novák, M. Wagner, C. Veit, K.-C. Möller, J. Besenhard, M. Winter, M. Wohlfahrt-Mehrens, C. Vogler, A. Hammouche, J. Power Sources 147 (1–2) (2005) 269–281.
[12] J. Li, E. Murphy, J. Winnick, P.A. Kohl, J. Power Sources 102 (2001) 294–301.
[13] G. Ning, B. Haran, B.N. Popov, J. Power Sources 117 (2003) 160–169.
[14] J. Gerschler, D.U. Sauer, EET-2007 European Ele-Drive Conference, Bruxelles, 2007.
[15] M. Broussely, S. Herreyre, P. Biensan, P. Kasztejna, K. Nechev, R.J. Staniewicz, J. Power Sources 97–98 (2001) 13–21.
[16] M. Andrew, CARB ZEV Symposium, Johnson Controls/Saft (2006).
[17] V.H. Johnson, A.A. Pesaran, T. Sack, Conference Paper 17th Annual Electric Vehicle Symposium, Montreal, 2000, http://www.nrel.gov/docs/fy01osti/28716.pdf.
[18] E. Karden, S. Buller, R.W.D. Doncker, J. Power Sources 85 (1) (2000) 72–78.
[19] S. Buller, Aachener Beiträge des ISEA, Band 31, Shaker Verlag GmbH, Aachen, 2003.
[20] D. Linzen, Aachener Beiträge des ISEA, Band 43, Shaker Verlag GmbH, Aachen, 2006.